Journal of Materials Chemistry C

ROYAL SOCIETY OF CHEMISTRY

PAPER

View Article Online
View Journal

Cite this: DOI: 10.1039/d5tc02737c

Overcoming the 5% EQE ceiling in deep-blue fluorescent OLEDs with hybridized local and charge transfer featured phenanthroimidazole-carbazole emitters

P. Keerthika,[b] Ankit Kumar,[a] Amutha Selvaganesan,[b] Jangho Moon,[d] Venkatramaiah Nutalapati,*[bc] Jun Yeob Lee*[def] and Rajendra Kumar Konidena*[a]

The design and development of deep-blue fluorescent organic emitters with Commission Internationale de l'Eclairage (CIE_y) < 0.06 and external quantum efficiency (EQE) over ~5.0% remains an enduring focus in organic light-emitting diodes (OLEDs). Herein, we report two new deep-blue organic emitters based on phenanthroimidazole (PI) frameworks, functionalized at the N1 and C2 positions. Specifically, carbazole was introduced at the N1 position *via* its C3 site to enhance its hole-transporting ability and thermal stability, while either biphenyl (**PICz-BP**) or cyanophenyl (**PICz-CN**) was attached at the C2 position to extend π-conjugation and finely tune the photophysical properties. Photophysical studies revealed that both emitters exhibit deep-blue emission, with emission maxima (λ_{em}) of ~409 nm for **PICz-BP** and 419 nm for **PICz-CN**. The slightly red-shifted emission observed for **PICz-CN** is attributed to enhanced charge-transfer character induced by the electron-withdrawing cyano group. Furthermore, solvatochromic studies and computational analysis revealed that both compounds exhibit hybridized local and charge-transfer (HLCT) excited states, a feature known to enhance radiative decay while maintaining high color purity. Both emitters displayed high photoluminescence quantum yields (PLQYs) and good thermal stability, making them promising candidates for organic light emitting diodes (OLEDs). Their performance was evaluated in both doped and non-doped OLED devices. Notably, the doped device employing **PICz-BP** achieved excellent performance, delivering a maximum EQE of 6.1% with deep-blue emission ($CIE_y \approx 0.06$). Remarkably, the non-doped device based on **PICz-BP** also retained comparable color purity and exhibited an EQE of 4.4%, underscoring the intrinsic emissive strength and stability of the material without the need for a host matrix. Overall, the successful design strategy leveraging HLCT character enabled both emitters to exhibit high EQE > 5%, highlighting their potential for high-performance deep-blue OLEDs.

Received 18th July 2025,
Accepted 21st August 2025

DOI: 10.1039/d5tc02737c

rsc.li/materials-c

Introduction

The establishment of clear structure–property relationships in organic luminescent materials remains a pivotal challenge and an enduring focus within the scientific community, driven by their broad applications in organic light-emitting diodes (OLEDs),[1–13] biomedical imaging,[14] chemical sensors,[15] and other optoelectronic devices.[16–18] Among these, OLEDs have attracted significant attention due to their merits such as high color purity, mechanical flexibility, low cost, and potential for rollable and lightweight displays.[19–23] In OLEDs, the organic emitters play a critical role in determining key device characteristics including emission color, spectral purity, charge transport, efficiency, and operational stability.[24–27] While efficient red and green emitters have reached commercial benchmarks,

[a] Organic Materials Laboratory (OML), Department of Chemistry, Indian Institute of Technology-Patna, Bihta Kanpa Rd, Dayalpur, Daulatpur, Patna, Bihar 801106, India. E-mail: rajsan@iitp.ac.in, rkonidena531@gmail.com
[b] Functional Materials Laboratory, Department of Chemistry, Faculty of Engineering and Technology, SRM Institute of Science and Technology, Kattankulathur, Chennai 603203, India. E-mail: venkatrv1@srmist.edu.in, nvenkat83@gmail.com
[c] Centre for Interdisciplinary Research (CIDR), SRM University-AP, Amaravati, Andhra Pradesh 522 240, India
[d] Department of Display Convergence Engineering, Sungkyunkwan University, 2066, Seobu-ro, Jangan-gu, Suwon, Gyeonggi, 16419, Republic of Korea. E-mail: leej17@skku.edu
[e] School of Chemical Engineering, Sungkyunkwan University, 2066, Seobu-ro, Jangan-gu, Suwon, Gyeonggi, 16419, Korea
[f] SKKU Institute of Energy Science and Technology, Sungkyunkwan University, 2066, Seobu-ro, Jangan-gu, Suwon, Gyeonggi, 16419, Korea

the development of high-performance deep-blue emitters remains a formidable task.[9,28–31] Specifically, achieving deep-blue emission with Commission Internationale de l'Éclairage (CIE) coordinates of (0.15, 0.06), as defined by HDTV standard ITU-R and the NTSC standard, along with an external quantum efficiency (EQE) greater than 5%, continues to be a significant bottleneck.[28–31] Deep-blue emitters are not only essential as one of the primary colors for full-color displays, but also serve as host materials for low-energy dopants in white OLEDs and other applications.[32–41] Over the years, extensive research has been devoted to developing efficient deep-blue triplet-harvesting emitters, primarily *via* two approaches: metal-based phosphorescent OLEDs (PhOLEDs) and metal-free thermally activated delayed fluorescence (TADF) materials.[42] Both strategies offer 100% internal quantum efficiency by harvesting singlet and triplet excitons.[23,43–45]

However, deep-blue emission remains a challenge for both. In PhOLEDs, tuning the metal-to-ligand charge transfer (MLCT) transition to the deep-blue region often results in non-radiative decay pathways, severely limiting the photoluminescence quantum yield (PLQY).[46,47] Similarly, TADF materials based on donor–acceptor (D–A) architectures tend to produce broad emissions at longer wavelengths due to pronounced intramolecular charge transfer (ICT), and often suffer from efficiency roll-off due to the long-lived triplet excited states.[23,26,44,45] An alternative strategy that has emerged to mitigate these drawbacks is the design of emitters featuring a hybridized local and charge transfer (HLCT) excited state. In HLCT systems, the locally excited (LE) π–π* state contributes to high PLQY, while the charge transfer (CT) component facilitates triplet exciton harvesting through hot-exciton reverse intersystem crossing (hRISC).[37,48–50] This design balance allows for narrowband, efficient, and stable emission. Several HLCT emitters have demonstrated deep-blue emission with EQEs exceeding the limit of first generation fluorescent emitters (>5%) and reduced efficiency roll-off. However, such materials achieving both $CIE_y \leq 0.06$ and EQE > 6% remain rare.[51–54] The performance of HLCT emitters is highly sensitive to the choice of molecular building blocks and the mode of conjugation. Phenanthroimidazole (PI) is a well-established chromophore used in HLCT design, known for its rigid structure and favourable optoelectronic properties.[55–65] Carbazole, another widely adopted unit, offers excellent thermal and oxidative stability, along with hole-transporting ability.[66–68] While a few HLCT emitters combining PI and carbazole have been reported, direct linkage of carbazole at the C3-position to the N1-position of PI remains unexplored.

We hypothesized that this connectivity could introduce a large dihedral angle between the two units, spatially isolating the carbazole moiety. As a result, the carbazole would primarily serve as a hole-transporting and thermally stabilizing component without significantly altering the emission wavelength or HLCT behavior. Additionally, we postulated that modification at the C2-position of PI with biphenyl or cyanobenzene groups could modulate π-conjugation and fine-tune the emission properties and HLCT emission. To test this hypothesis, we designed and synthesized two new HLCT-deep-blue emitters, namely 2-([1,1′-biphenyl]-4-yl)-1-(9-ethyl-9*H*-carbazol-3-yl)-1*H*-phenanthro[9,10-*d*]imidazole (**PICz-BP**) and 4-(1-(9-ethyl-9*H*-carbazol-3-yl)-1*H*-phenanthro[9,10-*d*]imidazole-2-yl)benzonitrile (**PICz-CN**). Both emitters exhibited deep-blue emission (λ_{PL} < 419 nm) and wide optical bandgaps. **PICz-CN** showed a ~10 nm red-shift in emission compared to **PICz-BP**, attributed to enhanced ICT between the PI and CN acceptor. Thermal gravimetric analysis (TGA) revealed excellent thermal stability for both compounds, with **PICz-CN** exhibiting superior decomposition temperature due to the robustness of the CN unit. Photophysical, solvatochromic, and computational studies confirmed the HLCT characteristics and the potential for efficient triplet exciton utilization. OLED devices were fabricated in both doped and non-doped configurations. In doped devices, both the compounds displayed EQE > 5% attributed to the HLCT mechanism. Among them, the doped device based on **PICz-BP** exhibited the best performance, with a maximum EQE of 6.1% and deep-blue color purity ($CIE_y \approx 0.06$). Notably, its non-doped device retained comparable color purity ($CIE_y \approx 0.06$) and an EQE of 4.4%, indicating excellent emitter performance without the need for a host matrix. These results highlight the effectiveness of our molecular design strategy and suggest that the integration of carbazole and phenanthroimidazole through rationally chosen linkages and substitutions offers a promising path toward high-performance, deep-blue OLED emitters.

Results and discussion

Molecular design and synthesis

The primary objective of this work is to develop pure deep-blue emitters with EQE > 5% and CIE_y < 0.06 by structurally modifying PI at the N1-position with a rigid carbazole unit *via* C3-connectivity, and extending conjugation through the C2-position using biphenyl or cyanophenyl groups. It is anticipated that the bulky carbazole unit at the N1-position will introduce significant steric hindrance, causing it to twist out of the PI plane and become de-conjugated from PI. As a result, carbazole integration is expected to have minimal impact on the emission wavelength, while enhancing thermal stability and hole- transporting properties. In contrast, the extended π-conjugation through the biphenyl group at the C2-position is expected to induce a long-axis LE state (Fig. 1). Additionally, substituting one phenyl ring with a cyano (–CN) group is aimed at balancing the charge transport characteristics of the emitter. Scheme 1 illustrates the synthetic routes for the two target compounds, **PICz-BP** and **PICz-CN**. The key intermediate, PICz-Br, was synthesized *via* the Debus–Radziszewski imidazole synthesis, as reported in the literature.[69,70] **PICz-BP** was then obtained by Pd-catalysed Suzuki–Miyaura cross-coupling[71] of PICz-Br with phenylboronic acid. **PICz-CN** was synthesized *via* cyanation of PICz-Br using copper(I) cyanide (CuCN) in *N*,*N*′-dimethylformamide (DMF) under reflux conditions. The desired compounds were purified by column chromatography followed by recrystallization. The chemical structures of the

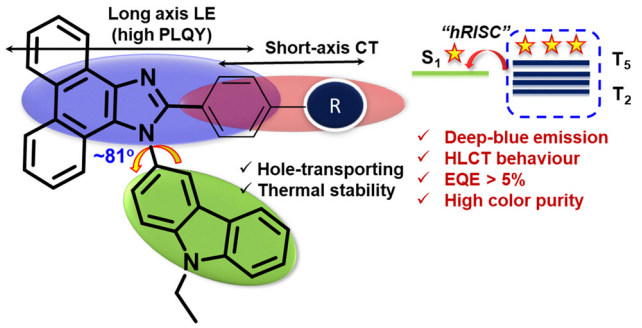

Fig. 1 Molecular design of the PICz-based deep-blue HLCT emitters.

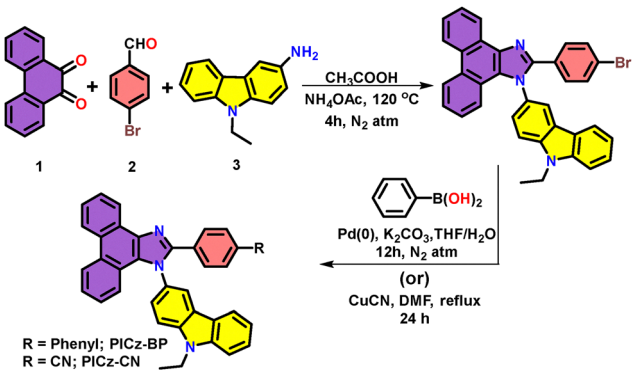

Scheme 1 Synthetic route for the compounds **PICz-BP** and **PICz-CN**.

synthesized compounds were confirmed by ^{1}H and ^{13}C Nuclear Magnetic Resonance (NMR) spectroscopy and high-resolution mass spectrometry (HRMS). For OLED applications, the final compounds were further purified by vacuum train sublimation to ensure high purity (>99%) for device fabrication.

Theoretical studies

Computational studies were carried out to investigate the relationship between the molecular geometry and optical properties of the compounds, and to gain insight into the electronic distribution, particularly the frontier molecular orbitals (FMOs), *i.e.*, the highest occupied molecular orbital (HOMO) and the lowest unoccupied molecular orbital (LUMO). Geometry optimizations were performed in the gas phase using density functional theory (DFT) and Time-dependent density functional theory (TD-DFT) as implemented in the Gaussian 09 software package, employing Becke's three-parameter hybrid functional (B3LYP) with the 6-31G(d,p) basis set.[72] The optimized molecular geometries with the spatial distributions of the HOMO and LUMO orbitals and energy level diagram for singlet (S_n) and triplet (T_n) excited states are presented in Fig. 2. The HOMO orbitals are primarily delocalized along the PI core and marginally extended onto the biphenyl or cyanophenyl moieties, which can be attributed to the relatively small dihedral angle between the phenyl and imidazole units. In contrast, the LUMO orbitals are mainly localized on the biphenyl or cyanophenyl units, with minor contributions from the PI core. This partial spatial separation of the HOMO and LUMO indicates a HLCT character in these molecules (*vide infra*). Importantly, the carbazole unit exhibits minimal involvement in either the HOMO or LUMO, owing to its large dihedral angle (~81°) between the carbazole and PI core. This implies that the carbazole moiety does not significantly influence the emission wavelength but contributes to enhanced thermal stability and hole-transporting characteristics. The theoretically calculated HOMO/LUMO energy levels and electronic bandgaps (E_g) for **PICz-BP** and **PICz-CN** are −5.67/−1.67/4.0 eV and −5.70/−2.08/3.62 eV, respectively. Notably, **PICz-BP** exhibits a wider bandgap, suggesting a more blue-shifted emission compared to its congener **PICz-CN**, thereby supporting its potential for deep-blue emission in OLED applications. Furthermore, Fig. 2c depicts the energy level diagram for singlet (S_n) and triplet (T_n) excited states of **PICz-BP** and **PICz-CN**, which shows that these fluorophores exhibit large $\Delta E_{S_1-T_1}$ (>0.5 eV), whereas ΔE_{ST} between the first excited singlet state (S_1) and high lying T_n (n = 4–5) states was found to be ≤0.1 eV. Therefore, these molecules are expected to exhibit efficient high-lying reverse intersystem crossing (hRISC) *via* a hot exciton process, leading to HLCT emission. Furthermore, the estimated spin–orbit coupling (SOC) constants between the S1 and T2, T3, T4 and T5-states of the compounds are large enough to facilitate hRSIC.[73,74]

Thermal and electrochemical properties

The thermal stability of the emitters was evaluated using TGA and differential scanning calorimetry (DSC) methods, conducted under a nitrogen atmosphere at a heating rate of 10 °C min^{-1}. The corresponding TGA and DSC thermograms are presented in Fig. S1 and S2. As anticipated, both **PICz-BP** and **PICz-CN** demonstrated excellent thermal stability, with decomposition temperatures (T_{10d}, defined as the temperature at 10% weight loss) of 330 °C and 369 °C, respectively. Notably, **PICz-BP** exhibited enhanced thermal stability compared to PIBP, highlighting the positive effect of carbazole incorporation on the thermal robustness of PICz-based HLCT emitters. In addition, both compounds showed high glass transition temperatures (T_g), measured at 226 °C for **PICz-BP** and 303 °C for **PICz-CN**, indicating superior morphological stability. These thermal properties make them promising candidates for stable and efficient OLED applications.

To investigate the redox behaviour of these compounds, cyclic voltammetry (CV) measurements were carried out using dilute dichloromethane solutions of the emitters. Ferrocene/ferrocenium (Fc/Fc^+) was used as an internal standard, and tetrabutylammonium perchlorate (TBAP) served as the supporting electrolyte. The cyclic voltammograms are shown in Fig. S3. Both compounds exhibited two or more oxidation waves, with oxidation potentials shifted positively relative to ferrocene. These shifts are attributed to the removal of electrons from either the carbazole unit or the PI conjugated core. Among the

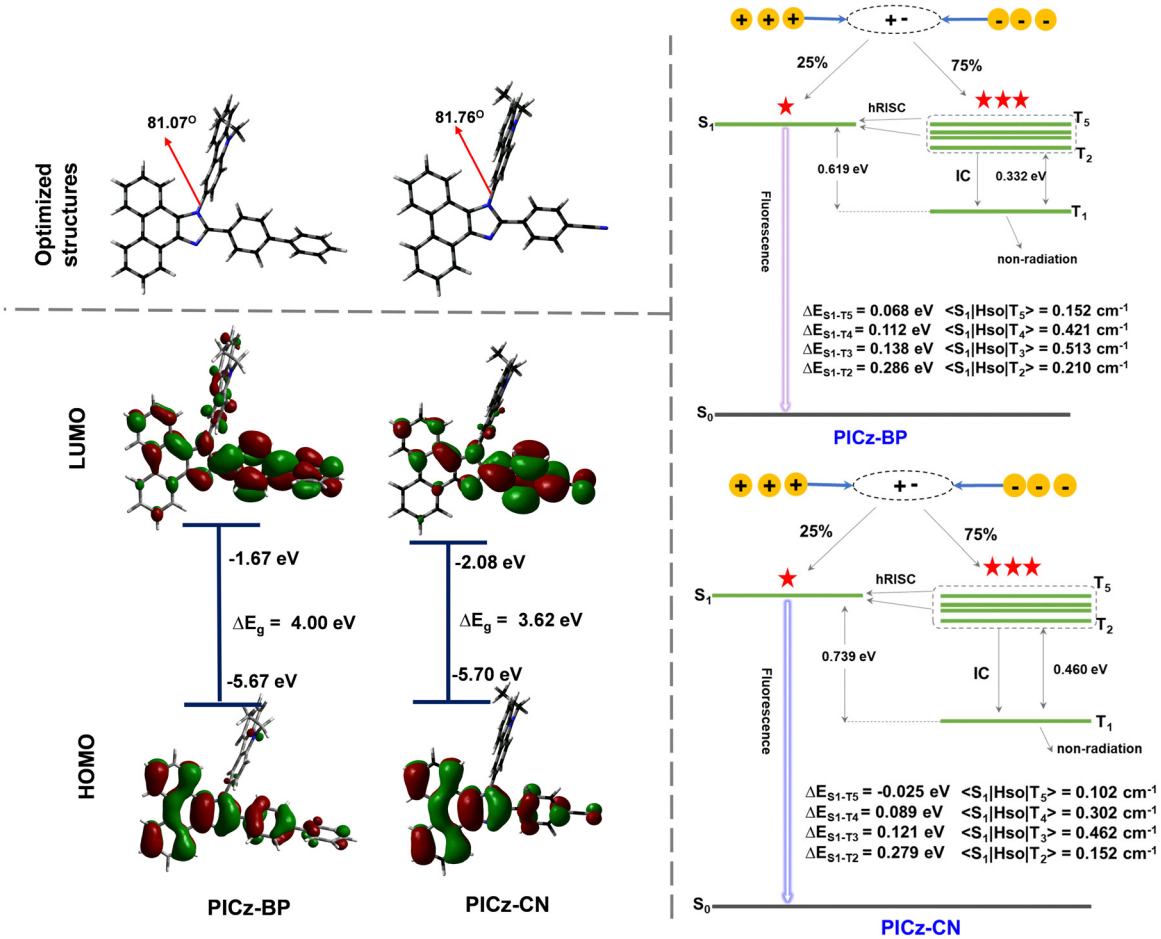

Fig. 2 (a) Optimized geometries, (b) FMO distribution of **PICz-BP** and **PICz-CN** computed by the DFT method, and (c) energy level diagram for singlet (S_n) and triplet (T_n) excited states of **PICz-BP** and **PICz-CN** calculated by B3LYP/631-G(d,p).

two, **PICz-BP** exhibited a lower oxidation potential than **PICz-CN**, which can be ascribed to the higher electron-donating nature of the PI–biphenyl conjugate system compared to the PI-cyanophenyl system. The HOMO energy levels of **PICz-BP** and **PICz-CN** were estimated using standard empirical methods and found to be −5.87 eV and −5.91 eV, respectively. The LUMO energy levels were calculated by subtracting the optical bandgap from the corresponding HOMO values, yielding −2.33 eV for **PICz-BP** and −2.70 eV for **PICz-CN**. The lower LUMO level of **PICz-CN** is attributed to the electron-withdrawing effect of the CN group. Overall, the trends observed in the experimentally derived HOMO, LUMO, and E_g values are consistent with theoretical calculations, with minor discrepancies attributed to solute–solvent interactions during experimental measurements.

Photophysical properties

The photophysical properties of the compounds were investigated using UV-visible absorption and photoluminescence (PL) spectroscopy. Fig. 3a presents the absorption and emission spectra recorded in dilute toluene solutions, and the relevant photophysical data are summarized in Table 1. Both compounds exhibit multiple absorption bands in the range of 290–400 nm. The high-energy bands below 300 nm are attributed to localized π–π* transitions of the carbazole and PI cores. In contrast, the absorption bands above 300 nm are assigned to delocalized π–π* transitions across the extended conjugated backbones or to partial ICT. While the overall absorption profiles of **PICz-BP** and **PICz-CN** are similar, the latter shows a slightly red-shifted absorption, which is attributed to the electron-withdrawing cyano group that enhances the ICT character compared to the phenyl-substituted **PICz-BP**. The PL spectra reveal that both compounds emit in the deep-blue region (<420 nm) with structured emission profiles, indicating that the emission primarily originates from the local excited (LE) state. **PICz-BP** and **PICz-CN** display emission maxima at 409 nm and 419 nm, respectively, with narrow FWHM ~56 nm. The 10 nm red-shift observed for **PICz-CN** is consistent with enhanced ICT from the PI donor to the cyano acceptor. The E_g values were estimated from the intersection of the normalized absorption and emission spectra, yielding values of 3.44 eV for **PICz-BP** and 3.21 eV for **PICz-CN**. The absolute PLQYs of the

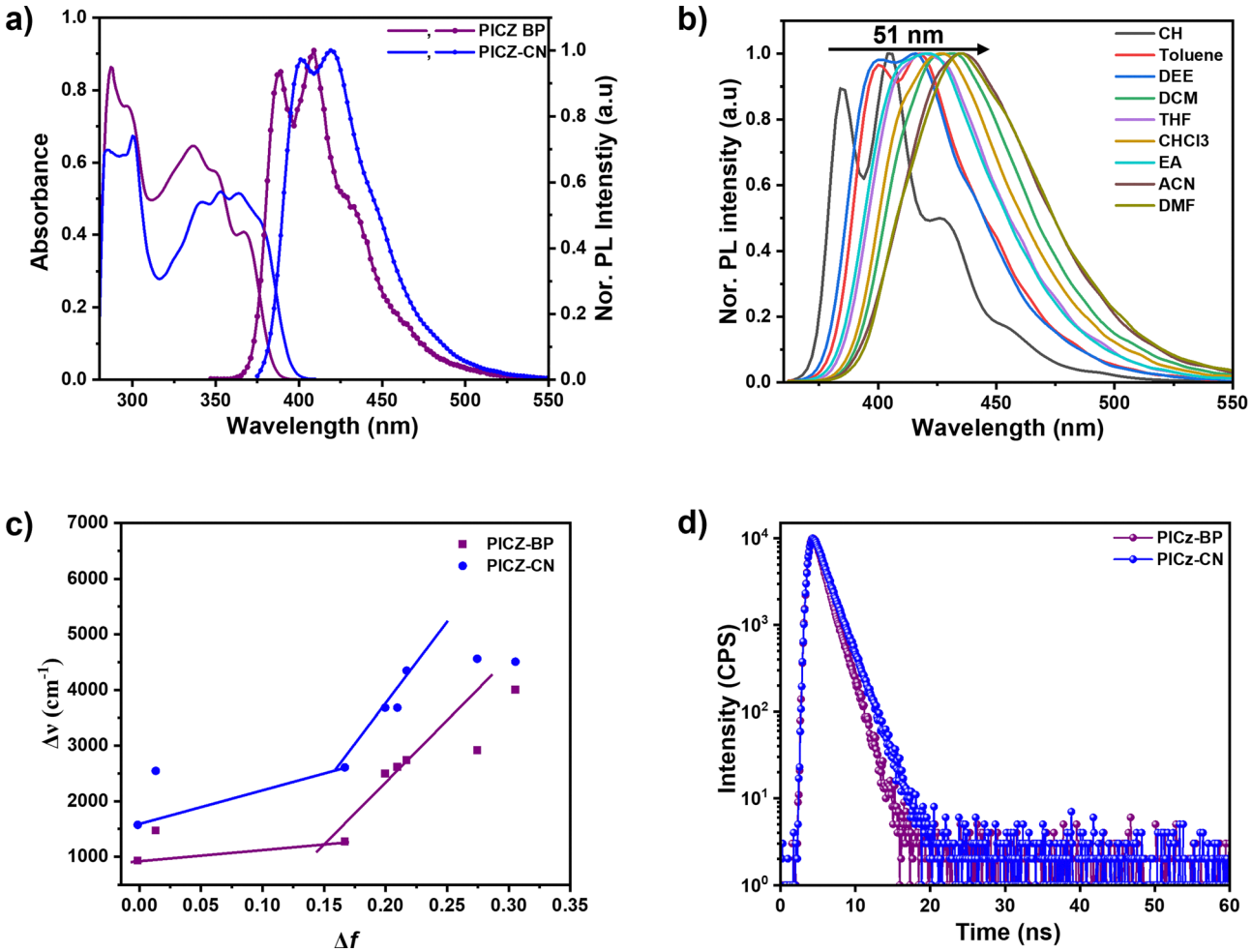

Fig. 3 (a) Absorption and emission spectra for the compounds in dilute toluene solution; (b) solvatochromic studies for the compound **PICz-CN**; (c) Lippert–Mataga plot; (d) Lifetime decay curve.

Table 1 Optical, electrochemical and thermal properties of the compounds

Compound	λ_{abs}[a], nm	λ_{pl}[a] sol/film (FWHM, nm)	PLQY[a] (%)	T_{10d}[b]/T_g (°C)	HOMO[cd] (eV)	LUMO[ce] (eV)	E_g[cf] (eV)	τ[g] (ns)	$S_1/T_1/\Delta E_{ST}$[h] (eV)
PICz-BP	299 337 367	409/419 (56/76)	95.6	330/226	−5.67/−5.87	−1.67/−2.33	4.00/3.34	2.09	3.26/3.00/0.26
PICz-CN	341 352 377	419/457 (56/87)	95.9	369/303	−5.70/−5.91	−2.08/−2.70	3.61/3.21	2.42	3.08/2.78/0.30

[a] Measured in dilute toluene solution. [b] Thermal decomposition temperature corresponds to 10% weight loss. [c] Calculated from DFT. [d] Estimated from CV. [e] Calculated by subtracting the HOMO from the optical band gap. [f] Optical band gap. [g] Excited state fluorescence lifetime. [h] Estimated from the fluorescence and phosphoresce spectra.

compounds, measured using an integrating sphere in dilute toluene, were remarkably high (~95–96%). The time-resolved fluorescence decay measurements revealed single exponential decay with lifetime (τ) in the nanosecond range (Fig. 3d). The CN derivative showed a relatively longer τ of 2.42 ns compared to the corresponding biphenyl derivative (τ = 2.09 ns), attributed to the enhanced CT component of the former, which is confirmed by solvatochromic studies. To examine the influence of solvent polarity on the ground and excited states, solvatochromism studies were performed in solvents of varying polarity, ranging from non-polar cyclohexane (CH) to polar acetonitrile (ACN) (Fig. 3b and Fig. S4). The absorption spectra showed no change on increasing solvent polarity, suggesting negligible non-polar ground state. In contrast, the emission spectra exhibited pronounced positive solvatochromism. As the solvent polarity increased, the structured vibronic features in non-polar solvents such as CH and toluene gradually became broader and red-shifted, indicating a transition from a non-polar LE state to a polar excited state. This red-shifted, featureless emission in polar solvents is typically attributed to CT-induced electronic perturbations in the excited state. Notably, large Stokes shifts observed in polar solvents further support the presence of a polar excited state. These results clearly indicate that the observed solvatochromism arises from photo-induced ICT from the PI core to the biphenyl or cyanophenyl moieties. **PICz-CN** displayed a large degree of bathochromic

shift (λ_{CH-ACN}) of 51 nm, confirming a strong ICT character, in agreement with DFT results. To further analyse the solvatochromic behaviour, the orientation polarizability (Δf) was correlated with the Stokes shift using the Lippert–Mataga model to estimate the excited-state dipole moments (Fig. 3c). Both compounds displayed a two-segment linear relationship across low- and high-polarity solvents. This observation suggests the hybridization of LE and CT components into a single emissive HLCT state, which is expected to enhance the EL performance of these materials. Furthermore, the computationally calculated higher triplet energy states (T_n, n = 1 to 4) closely resonate with the higher singlet state with E_{S1-T5}/E_{S1-T6} for **PICz-BP** of 0.06/0.07 eV and E_{S1-T3}/E_{S1-T4} of 0.02/0.08 eV for **PICz-BP**, which facilitates hot-exciton up conversion.

Electroluminescence properties

The deep-blue emission, high PLQY, and HLCT characteristics of **PICz-BP** and **PICz-CN** motivated us to explore their potential in OLED applications. To assess their electroluminescent performance, both non-doped and doped OLED devices were fabricated. Initially, the non-doped OLED device was fabricated with the configuration of PEDOT:PSS (40 nm)/TAPC (10 nm)/mCP (5 nm)/EML (30 nm)/TSPO1 (25 nm)/LiF (1.5 nm)/Al (200 nm), in which poly(3,4-ethylenedioxythiophene):poly(styrene sulfonate) (PEDOT:PSS) acts as a hole-injecting layer, di-(4-(*N*,*N*-ditolylamino)-phenyl)cyclohexane (TAPC) as a hole transporting layer and diphenyl[4-(triphenylsilyl)phenyl]phospine oxide (TSPO1) as an electron transporting layer. [9,9′]-, 1,3-bis-(carbazole-9-yl)benzene (mCP) was used as the exciton blocking layer. ITO and LiF/Al act as the cathode and anode, respectively. The energy level alignment and chemical structures of the layers are shown in Fig. 4a and 5a, while the current density–voltage–luminance (*J*–*V*–*L*) characteristics and electroluminescence (EL) spectra are presented in Fig. 4 and the corresponding summarized EL data are shown in Table 2. Among the devices, **PICz-CN** demonstrated higher current density and luminance than **PICz-BP**, likely due to its lower LUMO energy level and enhanced electron mobility imparted by the electron-withdrawing cyano group. The EL spectra revealed deep-blue to blue emissions with peak wavelengths/CIE(x,y) coordinates of 437 nm/(0.15, 0.06) for **PICz-BP** and 454 nm/(0.15, 0.12) for **PICz-CN**. The close resemblance of the EL to the PL spectra in solution suggests that the emission originates from the emitter molecules themselves, and that aggregation was effectively suppressed in the non-doped devices possibly due to the large dihedral angle between the carbazole and PI units. These non-doped devices exhibited EQE_{max}/current- efficiency (CE) of 4.4%/2.3 cd A^{-1} for **PICz-BP** and 4.1%/4.4 cd A^{-1} for **PICz-CN**, demonstrating promising EL performance. To further enhance device performance, doped OLEDs were fabricated using the modified configuration: PEDOT:PSS (40 nm)/TAPC (10 nm)/mCP (5 nm)/EML (30 nm)/TSPO1

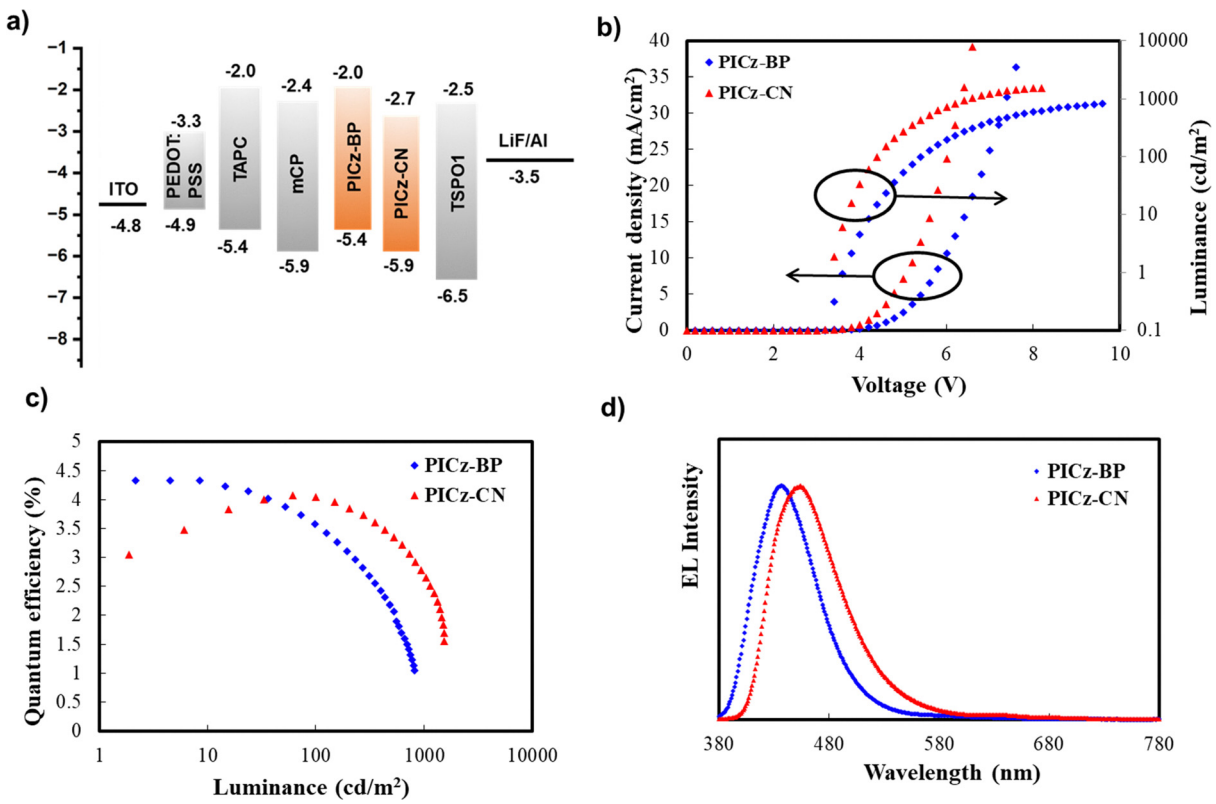

Fig. 4 (a) Non-doped OLED device structure and energy level diagram; (b) *I*–*V*–*L* plot; (c) EQE *vs.* *L* plot; (d) EL plot for the compounds in the non-doped OLED device.

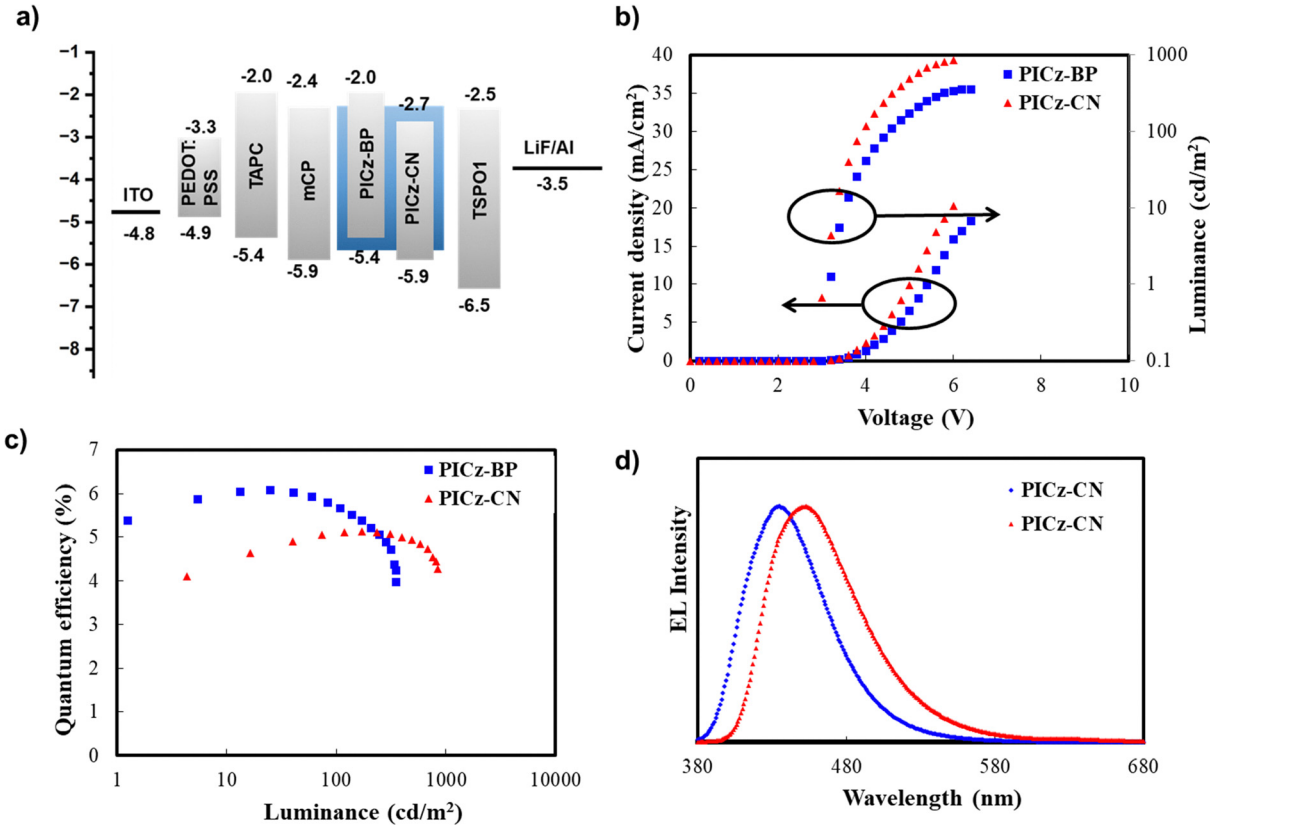

Fig. 5 (a) Doped OLED device structure and energy level diagram (host: PCzAc (Homo/LUMO ~ −5.7/−2.4)); (b) *I*–*V*–*L* plot; (c) EQE *vs.* *L* plot; (d) EL plot.

Table 2 Electroluminescence properties of the compounds

Device	Compound	Turn-on (V)	CE_{max} (cd A^{-1})	EQE_{max}/EQE_{1000} cd m^{-2} (%)	L_{max} (cd m^{-2})	EL_{max} (nm)	CIE (x,y)
Non-doped	**PICz-BP**	5.4	2.3	4.4/1.0	99.3	437	0.15,0.06
	PICz-CN	4.8	4.4	4.1/2.7	202.1	454	0.15,0.12
Doped							
	PICz-BP	4.8	3.2	6.1/4.0	138.4	438	0.15,0.06
	PICz-CN	4.5	5.3	5.1/4.3	259.1	453	0.15,0.12

CE_{max} = maximum current efficiency, EQE_{max} = maximum external quantum efficiency, L_{max} = maximum luminance.

(25 nm)/LiF (1.5 nm)/Al (200 nm), where the emitters **PICz-BP** and **PICz-CN** were doped into a PCzAC host matrix. The energy alignment, *J*–*V*–*L* curves, EL spectra, and EQE *vs.* L plots are shown in Fig. 5. Similar to the non-doped devices, **PICz-CN** exhibited higher *J* and *L*. The EL spectra showed pure deep-blue to blue emission with peak wavelengths of 438 nm for **PICz-BP** and 453 nm for **PICz-CN**. These closely match their PL spectra in solution, confirming that the EL emission originates from the dopant molecules. The absence of any additional peaks in the EL spectra further supports efficient energy transfer from host to guest and minimal exciton quenching. As anticipated, the doped OLEDs showed improved performance with EQE_{max} of 6.1% for **PICz-BP** and 5.1% for **PICz-CN**. These values surpass the EQE (5%) limit for purely fluorescent OLEDs, which is attributed to the contribution of triplet excitons *via* HLCT emission mechanisms (*vide supra*). Notably, both doped and non-doped devices based on **PICz-BP** achieved pure deep-blue emission with a CIE(x,y) coordinate of (0.15, 0.06), precisely matching with NTSC deep-blue coordinates. Overall, the doped device incorporating **PICz-BP** demonstrated the best performance, achieving an EQE_{max} of 6.1%, a CE of 3.2 cd A^{-1}, and a power efficiency (PE) of 2.9 lm W^{-1}. Furthermore, the operational lifetime of the devices was evaluated to assess their stability, and the relative luminance was plotted as a function of driving time (Fig. S7) with an initial luminance of 100 cd m^{-2}. Although the devices exhibited short lifetimes overall, the **PICz-CN**–based device demonstrated a comparatively longer lifetime of 0.76 h than **PICz-BP**, which can be attributed to its superior chemical robustness.

Conclusions

In summary, we have successfully designed and synthesized two new deep-blue organic emitters based on PI frameworks, strategically functionalized at the N1 and C2 positions.

Incorporation of carbazole at the N1 position enhanced hole-transporting ability and thermal stability, while the introduction of biphenyl (**PICz-BP**) or cyanophenyl (**PICz-CN**) at the C2 position effectively extended π-conjugation and fine-tuned the photophysical properties. Both emitters exhibited deep-blue emission with $\lambda_{em} < 419$ nm, where the slight red-shift in **PICz-CN** was originated from increased ICT due to the cyano group. Solvatochromic studies and theoretical calculations confirmed that both compounds exhibit HLCT excited states. The materials also exhibited high PLQY and excellent thermal stability, validating their suitability for OLED applications. Device evaluations further demonstrated their potential: the doped OLED based on **PICz-BP** achieved an impressive EQE_{max} of 6.1% with deep-blue emission ($CIE_y \approx 0.06$), while the non-doped device maintained comparable color purity and still reached a notable EQE of 4.4%. These results underscore the effectiveness of our molecular design strategy leveraging HLCT character to develop deep-blue emitters with EQE > 5%, highlighting **PICz-BP** and **PICz-CN** as promising candidates for high-efficiency deep-blue OLEDs.

Author contributions

Keerthika P.: conceptualization and synthesis of materials; Amutha Selvaganesan and Ankit Kumar: supporting in analysis; Jangho Moon: OLED device fabrication and testing; Venkatramaiah Nutalapati: conceptualization, supervision, funding acquisition, and project administration; Jun Yeob Lee: conceptualization, supervision and writing & editing the manuscript; Rajendra Kumar Konidena conceptualization, supervision, funding acquisition, and project administration.

Conflicts of interest

There are no conflicts to declare.

Data availability

The data supporting this article have been included as part of the SI. Supplementary Information: Experimental section, NMR, Photophysical properties, CV, TGA, DSC, EL data and Cartesian coordinates. See DOI: **https://doi.org/10.1039/d5tc02737c**.

Acknowledgements

V. Nutalapati, Keerthika P. and A. S. acknowledge SRMIST for providing sophisticated analytical facilities and HPCC support for characterization. Keerthika P. and A. S. thank SRMIST for the PhD fellowship. A. K. thank IIT-Patna for institute fellowship for Ph.D. R. K. Konidena acknowledge the SAIF facility, IIT Patna and Synthenta Pvt. Ltd. for funding this research. J. Y. Lee acknowledges MOTIE (20022488, RS-2024-00418086).

Notes and references

1 C. W. Tang and S. A. VanSlyke, *Appl. Phys. Lett.*, 1987, **51**, 913–915.
2 A. P. Kulkarni, C. J. Tonzola, A. Babel and S. A. Jenekhe, *Chem. Mater.*, 2004, **16**, 4556–4573.
3 Y.-C. M. Wu, M. F. Molaire, D. S. Weiss, F. A. Angel, C. R. DeBlase and B. P. Fors, *J. Org. Chem.*, 2015, **80**, 12740–12745.
4 K. R. Justin Thomas, J. T. Lin, Y.-T. Tao and C.-W. Ko, *J. Am. Chem. Soc.*, 2001, **123**, 9404–9411.
5 S. Y. Lee, T. Yasuda, Y. S. Yang, Q. Zhang and C. Adachi, *Angew. Chem., Int. Ed.*, 2014, **53**, 6402–6406.
6 Y. Shirota, *J. Mater. Chem.*, 2000, **10**, 1–25.
7 M. A. Baldo, M. E. Thompson and S. R. Forrest, *Nature*, 2000, **403**, 750–753.
8 X.-H. Zhu, J. Peng, Y. Cao and J. Roncali, *Chem. Soc. Rev.*, 2011, **40**, 3509.
9 M. Zhu and C. Yang, *Chem. Soc. Rev.*, 2013, **42**, 4963.
10 S. Kumar, M. Singh, J.-H. Jou and S. Ghosh, *J. Mater. Chem. C*, 2016, **4**, 6769–6777.
11 Z. Zhou, Q. Li, L. Chen, C. Liu and S. Fan, *J. Mater. Chem. B*, 2016, **4**, 1228–1234.
12 S. Jhulki, S. Seth, A. Ghosh, T. J. Chow and J. N. Moorthy, *ACS Appl. Mater. Interfaces*, 2016, **8**, 1527–1535.
13 J. Luo, S. Gong, Y. Gu, T. Chen, Y. Li, C. Zhong, G. Xie and C. Yang, *J. Mater. Chem. C*, 2016, **4**, 2442–2446.
14 C. Murawski and M. C. Gather, *Adv. Opt. Mater.*, 2021, **9**, 2100269.
15 T. M. Swager and K. A. Mirica, *Chem. Rev.*, 2019, **119**, 1–2.
16 Y. Wu and W. Zhu, *Chem. Soc. Rev.*, 2013, **42**, 2039–2058.
17 Y. Lin, Y. Li and X. Zhan, *Chem. Soc. Rev.*, 2012, **41**, 4245.
18 M. Mas-Torrent and C. Rovira, *Chem. Soc. Rev.*, 2008, **37**, 827.
19 Z. Zhu, J. Tan, W. Chen, Y. Yuan, L. Fu, C. Cao, C. You, S. Ni, Y. Chi and C. Lee, *Adv. Funct. Mater.*, 2021, **31**, 2102787.
20 X. Cai and S. Su, *Adv. Funct. Mater.*, 2018, **28**, 1802558.
21 L.-K. Li, C. C. Au-Yeung, M.-C. Tang, S.-L. Lai, W.-L. Cheung, M. Ng, M.-Y. Chan and V. W.-W. Yam, *Mater. Horiz.*, 2022, **9**, 281–293.
22 C. Poriel, J. Rault-Berthelot and D. Thirion, *J. Org. Chem.*, 2013, **78**, 886–898.
23 P. Rajamalli, N. Senthilkumar, P.-Y. Huang, C.-C. Ren-Wu, H.-W. Lin and C.-H. Cheng, *J. Am. Chem. Soc.*, 2017, **139**, 10948–10951.
24 Y. Kondo, K. Yoshiura, S. Kitera, H. Nishi, S. Oda, H. Gotoh, Y. Sasada, M. Yanai and T. Hatakeyama, *Nat. Photonics*, 2019, **13**, 678–682.
25 I. S. Park, M. Yang, H. Shibata, N. Amanokura and T. Yasuda, *Adv. Mater.*, 2022, **34**, 2107951.
26 H. Uoyama, K. Goushi, K. Shizu, H. Nomura and C. Adachi, *Nature*, 2012, **492**, 234–238.
27 Y. Xu, P. Xu, D. Hu and Y. Ma, *Chem. Soc. Rev.*, 2021, **50**, 1030–1069.
28 X. Yang, X. Xu and G. Zhou, *J. Mater. Chem. C*, 2015, **3**, 913–944.

29 G. Valchanov, A. Ivanova, A. Tadjer, D. Chercka and M. Baumgarten, *Org. Electron.*, 2013, **14**, 2727–2736.
30 W. Li, L. Yao, H. Liu, Z. Wang, S. Zhang, R. Xiao, H. Zhang, P. Lu, B. Yang and Y. Ma, *J. Mater. Chem. C*, 2014, **2**, 4733–4736.
31 P. Keerthika, A. Kumar, A. Maruthapillai, V. Nutalapati and R. K. Konidena, *J. Photochem. Photobiol., C*, 2025, **63**, 100698.
32 Y. Fu, H. Liu, B. Z. Tang and Z. Zhao, *Nat. Commun.*, 2023, **14**, 2019.
33 H. Li, H. Yan, X. Zhang, K. Shi, C. Kuang, X. Zheng, Y. He, L. Meng, H. Xu, Z. Meng, C. Yan, G. Wei, Y. Zhu and H. Meng, *Chem. Eng. J.*, 2024, **486**, 150142.
34 G. Meng, D. Zhang, J. Wei, Y. Zhang, T. Huang, Z. Liu, C. Yin, X. Hong, X. Wang, X. Zeng, D. Yang, D. Ma, G. Li and L. Duan, *Chem. Sci.*, 2022, **13**, 5622–5630.
35 Z. Xiao, Y. Zou, Z. Chen, J. Miao, Y. Qiu, Z. Huang, X. Cao, X. Peng and C. Yang, *Adv. Mater.*, 2025, **37**, 2419601.
36 J. Hu, Y. Pu, F. Satoh, S. Kawata, H. Katagiri, H. Sasabe and J. Kido, *Adv. Funct. Mater.*, 2014, **24**, 2064–2071.
37 R. K. Konidena, K. R. Justin Thomas, D. Kumar Dubey, S. Sahoo and J.-H. Jou, *Chem. Commun.*, 2017, **53**, 11802–11805.
38 R. K. Konidena, S. Oh, S. Kang, S.-S. Park, H. Lee and J. Park, *J. Org. Chem.*, 2022, **87**, 6668–6679.
39 J. N. Moorthy, P. Venkatakrishnan, P. Natarajan, Z. Lin and T. J. Chow, *J. Org. Chem.*, 2010, **75**, 2599–2609.
40 W.-C. Chen, C.-S. Lee and Q.-X. Tong, *J. Mater. Chem. C*, 2015, **3**, 10957–10963.
41 R. Kim, S. Lee, K.-H. Kim, Y.-J. Lee, S.-K. Kwon, J.-J. Kim and Y.-H. Kim, *Chem. Commun.*, 2013, **49**, 4664.
42 S. Nasiri, M. Rabiei, H. Shaki, M. Hosseinnezhad, K. Kalyani, A. Palevicius, A. Vilkauskas, G. Janusas, V. Nutalapati, S. Kment and J. Michel Nunzi, *J. Photochem. Photobiol., A*, 2024, **447**, 115289.
43 Y. J. Cho, S. K. Jeon and J. Y. Lee, *Adv. Opt. Mater.*, 2016, **4**, 688–693.
44 Y. Im, S. Y. Byun, J. H. Kim, D. R. Lee, C. S. Oh, K. S. Yook and J. Y. Lee, *Adv. Funct. Mater.*, 2017, **27**, 1603007.
45 J. Lee, H.-F. Chen, T. Batagoda, C. Coburn, P. I. Djurovich, M. E. Thompson and S. R. Forrest, *Nat. Mater.*, 2016, **15**, 92–98.
46 H. Xu, R. Chen, Q. Sun, W. Lai, Q. Su, W. Huang and X. Liu, *Chem. Soc. Rev.*, 2014, **43**, 3259–3302.
47 P.-T. Chou, Y. Chi, M.-W. Chung and C.-C. Lin, *Coord. Chem. Rev.*, 2011, **255**, 2653–2665.
48 S. Zhang, L. Yao, Q. Peng, W. Li, Y. Pan, R. Xiao, Y. Gao, C. Gu, Z. Wang, P. Lu, F. Li, S. Su, B. Yang and Y. Ma, *Adv. Funct. Mater.*, 2015, **25**, 1755–1762.
49 S. Zhang, W. Li, L. Yao, Y. Pan, F. Shen, R. Xiao, B. Yang and Y. Ma, *Chem. Commun.*, 2013, **49**, 11302.
50 W. Li, D. Liu, F. Shen, D. Ma, Z. Wang, T. Feng, Y. Xu, B. Yang and Y. Ma, *Adv. Funct. Mater.*, 2012, **22**, 2797–2803.
51 B. Liu, Z.-W. Yu, D. He, Z.-L. Zhu, J. Zheng, Y.-D. Yu, W.-F. Xie, Q.-X. Tong and C.-S. Lee, *J. Mater. Chem. C*, 2017, **5**, 5402–5410.
52 W.-C. Chen, Y. Yuan, S.-F. Ni, Q.-X. Tong, F.-L. Wong and C.-S. Lee, *Chem. Sci.*, 2017, **8**, 3599–3608.
53 X. Tang, Q. Bai, Q. Peng, Y. Gao, J. Li, Y. Liu, L. Yao, P. Lu, B. Yang and Y. Ma, *Chem. Mater.*, 2015, **27**, 7050–7057.
54 T. Shan, Y. Liu, X. Tang, Q. Bai, Y. Gao, Z. Gao, J. Li, J. Deng, B. Yang, P. Lu and Y. Ma, *ACS Appl. Mater. Interfaces*, 2016, **8**, 28771–28779.
55 Z. Zhong, Z. Liu, X. Wang, D. Xiong, H. Li, X. J. Feng, Z. Zhao and H. Lu, *J. Mater. Chem. C*, 2023, **11**, 16271–16279.
56 S. Geng, Z. Liu, H. Li, Z. Zhong, X. J. Feng, Z. Zhao and H. Lu, *Adv. Opt. Mater.*, 2024, **12**, 2301344.
57 C. Du, H. Liu, Z. Cheng, S. Zhang, Z. Qu, D. Yang, X. Qiao, Z. Zhao and P. Lu, *Adv. Funct. Mater.*, 2023, **33**, 2304854.
58 L. Wu, J. Xu, Z. Zhang, W. Xue, T. Wang, C. Yan, J. He, Y. He, H. Yan and H. Meng, *Mater. Adv.*, 2022, **3**, 1729–1736.
59 J. Jayabharathi, S. Sivaraj, V. Thanikachalam and J. Anudeebhana, *Mater. Adv.*, 2021, **2**, 6388–6402.
60 J. Xin, Z. Li, Y. Liu, D. Liu, F. Zhu, Y. Wang and D. Yan, *J. Mater. Chem. C*, 2020, **8**, 10185–10190.
61 G. Chen, Z. Qiu, J.-H. Tan, W.-C. Chen, P. Zhou, L. Xing, S. Ji, Y. Qin, Z. Zhao and Y. Huo, *Dye. Pigment.*, 2021, **184**, 108754.
62 S. Tang, G. Yang, J. Zhu, X. He, J. Jian, F. Lu and Q. Tong, *Chem. – Eur. J.*, 2021, **27**, 9102–9111.
63 H. Liu, Q. Bai, L. Yao, H. Zhang, H. Xu, S. Zhang, W. Li, Y. Gao, J. Li, P. Lu, H. Wang, B. Yang and Y. Ma, *Chem. Sci.*, 2015, **6**, 3797–3804.
64 S. Rana, S. R. Nayak, A. Saenubol, V. Promarak, S. Patel and S. Vaidyanathan, *Adv. Funct. Mater.*, 2025, 2507011.
65 J. Tagare and S. Vaidyanathan, *J. Mater. Chem. C*, 2018, **6**, 10138–10173.
66 R. K. Konidena, K. R. J. Thomas and J. W. Park, *ChemPhotoChem*, 2022, **6**, e202200059.
67 R. K. Konidena, K. R. Justin Thomas, S. Sahoo, D. K. Dubey and J.-H. Jou, *J. Mater. Chem. C*, 2017, **5**, 709–726.
68 R. K. Konidena, K. R. J. Thomas, S. Kumar, Y.-C. Wang, C.-J. Li and J.-H. Jou, *J. Org. Chem.*, 2015, **80**, 5812–5823.
69 Z. Wang, P. Lu, S. Chen, Z. Gao, F. Shen, W. Zhang, Y. Xu, H. S. Kwok and Y. Ma, *J. Mater. Chem.*, 2011, **21**, 5451.
70 E. Gelens, F. J. J. De Kanter, R. F. Schmitz, L. A. J. M. Sliedregt, B. J. Van Steen, C. G. Kruse, R. Leurs, M. B. Groen and R. V. A. Orru, *Mol. Divers.*, 2006, **10**, 17–22.
71 N. Miyaura, K. Yamada and A. Suzuki, *Tetrahedron Lett.*, 1979, **20**, 3437–3440.
72 M. J. Frisch, *Gaussian 09, Revision A.02*, Gaussian Inc., Wallingford, CT, 2009.
73 Y. Du, Y. Peng, W. Dong, H. Xu, X. Li, K. Chen, F. Wang, Y. Miao, P. Tao, H. Wang and J. Yu, *Chem. Sci.*, 2025, **16**, 14342.
74 S. Rana, S. R. Nayak, A. Saenubol, V. Promarak, S. Patel and S. Vaidyanathan, *Adv. Funct. Mater.*, 2025, 2507011.